

Starbursts hiding in the main sequence: a pathway toward quenching?

F. RENAUD^{1,2}, K. KRALJIC¹, J. FREUNDLICH¹, B. MAGNELLI³, M. BÉTHÉRMIN¹, C. ACCARD¹,
D. ISMAIL¹, E. DADDI³, D. ELBAZ³, L. CIESLA⁴, G. MARTIN⁵, Y. DUBOIS⁶, S. PEIRANI^{7,8,6}

¹ *Observatoire Astronomique de Strasbourg, Université de Strasbourg, CNRS UMR 7550, 11 rue de l'Université, F-67000 Strasbourg, France*

² *University of Strasbourg Institute for Advanced Study, 5 allée du Général Rouvillois, F-67083 Strasbourg, France*

³ *Laboratoire AIM Paris-Saclay, CEA/IRFU/Sap, Université Paris Diderot, F-91191 Gif-sur-Yvette Cedex, France*

⁴ *Aix Marseille Université, CNRS, LAM (Laboratoire d'Astrophysique de Marseille), 13388 Marseille, France*

⁵ *School of Physics and Astronomy, University of Nottingham, University Park, Nottingham NG7 2RD, UK*

⁶ *Institut d'Astrophysique de Paris, CNRS and Sorbonne Université, UMR 7095, 98 bis Boulevard Arago, F-75014 Paris, France*

⁷ *ILANCE, CNRS – University of Tokyo International Research Laboratory, Kashiwa, Chiba 277-8582, Japan*

⁸ *Kavli IPMU (WPI), UTIAS, The University of Tokyo, Kashiwa, Chiba 277-8583, Japan*

ABSTRACT

Star-forming galaxies spend most of their lifetimes on the star-forming main sequence, which establishes a tight empirical and statistical relation between stellar mass and star-formation rate. Occasional episodes of rapid star formation can push them temporarily above this sequence, turning them into starbursts. Yet some galaxies display starburst-like traits –rapid, dense, and compact star formation– while still remaining within the scatter of the main sequence. These “starbursts in the main sequence” (SBMSs) reveal the complexity and diversity of star formation modes, making them crucial for understanding how galaxies evolve and transition between different regimes. In this paper, we identify SBMSs in the cosmological simulation NEWHORIZON and follow their evolution across time to uncover their physical origins and the role of this special regime in shaping galaxy evolution. We explain the existence of SBMSs by a comparatively earlier assembly of their stellar mass, driven in particular by more frequent and repeated mergers as the other galaxies, as well as exceptionally productive starburst events triggered by these interactions. As a result, this regime appears preferentially –though not exclusively– in the most massive galaxies. The SBMS behavior is not continuous within individual galaxies but instead arises intermittently as a short-lived (~ 30 Myr) evolutionary mode. Nevertheless, such SBMS episodes exist throughout cosmic time across the galaxy population, rooted in the inherently stochastic nature of galactic star formation histories. Contrary to common interpretations in the literature, the SBMS phase marks a transition between starburst and more quiescent star formation in only a small fraction of cases ($< 25\%$). Compaction events do raise the star formation rate, but do not reduce the gas depletion time, i.e., the timescale for star formation. We find no evidence linking the SBMS regime to quenching via compaction (i.e., the blue-then-red-nugget pathway). The importance of the SBMS regime and the variety of evolutionary tracks into and out of it challenges attempts to summarize the evolution of star-forming galaxies with a single, universal scenario.

1. INTRODUCTION

The star formation rate (SFR) of galaxies has been empirically found to correlate with their stellar masses, along a relation called the main sequence of galaxy formation (Noeske et al. 2007; Elbaz et al. 2007; Daddi et al. 2007). Although this relation evolves with redshift (Whitaker et al. 2014; Speagle et al. 2014), it remains remarkably tight across cosmic time and stellar mass. The rare outliers with an excess of SFR for their mass (i.e., above the main sequence) are commonly referred to as starbursts, denoting an abnormal and likely short-lived activity, often ascribed to galaxy mergers (Rodighiero et al. 2011; Elbaz et al. 2011; Schreiber et al. 2015, but see Renaud et al. 2022 on mergers not triggering starbursts, and Liu et al. 2025 on nuclear starbursts not triggered by mergers). Despite their high productivity, the rarity of starbursts indicates that most stars do not form in this regime (Rodighiero et al. 2011). Conversely, galaxies below the main sequence are often interpreted as being on a pathway toward quenching with a possibility of later rejuvenation (Mancini et al. 2019).

Statistical analyses of large surveys of galaxy populations, probed notably in the submillimetric and millimetric domains with ALMA, have revealed the existence of a hybrid category of galaxies with gas depletion times as short as those of star-

bursts, but lying within the scatter of the main sequence. These “starbursts in the main sequence” (SBMSs) exhibit compact dust and radio emission, elevated dust temperatures, and extreme far-infrared surface brightness (Elbaz et al. 2018; Jiménez-Andrade et al. 2019; Puglisi et al. 2019, 2021), especially at the high-mass end (Gómez-Guijarro et al. 2022). All these aspects suggest a classification as starbursts, which is apparently incompatible with their belonging to the main sequence. The discovery of this population unveils a greater diversity (and likely complexity) in the regimes of star formation and the underlying physics of the main sequence. Among other questions, it raises the problem of transitions between star formation regimes, and whether such evolutions are quasi-adiabatic and smooth, or require a sudden shift in environmental conditions.

Magnelli et al. (2023) used MIRI/JWST data up to cosmic noon ($z \approx 2$) to find that a significant fraction of the main sequence galaxies displays a compact, dust-obscured starburst-like star forming region, but embedded in a larger stellar component. Lyu et al. (2025) further classified these galaxies as “extended-compact”, representing 15% of their sample but being twice as common among massive galaxies. They postulate that these galaxies could be the progenitors of “compact-compact” systems, for which both the star-forming and old stellar components

appear compact, and perhaps on their way to becoming quiescent after a merger-triggered starburst phase (Puglisi et al. 2019; Tarrasse et al. 2025).

The enhancement of star formation activity during major mergers is not confined to the nucleus but rather spans large, kpc-scale volumes across the galaxy progenitors, including at high redshift (when resolved), as found observationally (e.g., Schweizer 2005; Whitmore et al. 2010; Mineo et al. 2014; Cortijo-Ferrero et al. 2017; Pan et al. 2019; Tsuge et al. 2020; Xu et al. 2021) and well reproduced in simulations (e.g., Di Matteo et al. 2008; Karl et al. 2010; Teyssier et al. 2010; Hopkins et al. 2013; Renaud et al. 2014, 2019b; Moreno et al. 2021; Li et al. 2022). However, the central concentration of dense gas – particularly during the last phases of interactions – leads to peaks of luminosity in the galactic nuclei (Mihos & Hernquist 1994; Ellison et al. 2025). This process is invoked to describe the first steps of the compaction mechanism in post-merger, coalesced, systems, i.e. the central concentration of star-forming material (Dekel & Burkert 2014; Puglisi et al. 2019; Lapiner et al. 2023), possibly in connection with the SBMS regime. Yet, Magnelli et al. (2023) noted that the diversity of galaxy populations could imply a variety of evolutionary pathways, which must be understood to decipher the histories of galaxies in and out of the main sequence (see also Arango-Toro et al. 2025; Tarrasse et al. 2025).

Toward this goal, Ciesla et al. (2023) proposed a quantification of the joint recent evolution of the SFR and the stellar mass. They employed spectral energy distribution (SED) fitting techniques to reconstruct the star formation history (SFH) of SBMSs identified as main sequence galaxies with dust-obscured, starburst-like activity in the GOODS-ALMA sample. They found no peculiarities in either the SEDs or the SFHs compared to other galaxies. Although SED fitting offers a unique access to the temporal dimension from observational data, parametric versions of this technique introduce artefacts by imposing the shape of the fitting functions (Ciesla et al. 2017; Iyer & Gawiser 2017; Lower et al. 2020). Even when describing the SFH piecewise (i.e., with a non-parametric or, more precisely, a non-analytical approach like in Ciesla et al. 2023; see also Ocvirk et al. 2006; Leja et al. 2019; Tacchella et al. 2020), SED fitting suffers from uncertainties in stellar evolution and dust models, as well as degeneracies in the solutions (Conroy 2013; Caplar & Tacchella 2019; Carvajal-Bohorquez et al. 2025).

In parallel, cosmological simulations are prime tools for understanding time evolutions and probing the diversity of histories among galaxies. Tacchella et al. (2016) used the VELA cosmological zoom-in simulations to confirm the process of compaction through the ignition of a central starburst (“blue nugget”), followed by the formation of a stellar core and quenching of star formation activity. The concentration of gas is caused by loss of angular momentum via gravitational torques from mergers, accretion from large scales, or the formation of massive clumps in disk instabilities (Lapiner et al. 2023). In the NEWHORIZON simulation, Martin et al. (2021) found that not all interaction-triggered enhancements of star formation would push the galaxies off the main sequence, especially at high redshift. However, the connection with the SBMS regime has not been explicitly studied, and hypotheses regarding the role of this regime in galaxy evolution remain highly speculative. Furthermore, although the high resolution of zoom-in simulations is essential to capture the physical conditions of star formation, it imposes limits on the modeled volume, and thus on the diversity of galaxies probed (as underlined in Zhang et al. 2025).

In this paper, we use the cosmological simulation NEWHORIZON (Dubois et al. 2021) to propose a theoretical ex-

planation for the nature and evolution of SBMS galaxies. This simulation combines a large volume, comprising a relatively wide diversity of galaxies, with the high resolution (≈ 34 pc) needed to (partially) capture the conditions of star formation within these galaxies. The starting point of our study is a necessary clarification of the terms and definitions used (Section 3). We then present a series of diagnostics relying on population statistics as well as individual evolutions, to illustrate the nature of SBMS galaxies (Section 4.1) and their possible evolution toward this peculiar regime (Sections 4.2 and 4.3). After discussing the limitations of our approach (Section 5), we summarize our theoretical picture of this phenomenon (Section 6).

2. METHOD

2.1. Simulation

We use the large-scale zoom-in cosmological simulation NEWHORIZON¹ presented in Dubois et al. (2021), and the selection of star-forming galaxies from Kraljic et al. (2024). We refer the reader to these papers for details, as only a summary is presented here. NEWHORIZON is run with the RAMSES code (Teyssier 2002), with mass resolutions of $1.2 \times 10^6 M_\odot$ and $1.3 \times 10^4 M_\odot$ for the dark matter and stellar particles, respectively. Hydrodynamics is solved using the adaptive mesh refinement technique down to a resolution of 34 pc in the densest regions, with heating from an ultraviolet background (Haardt & Madau 1996), self-shielding of optically thick regions (Rosdahl & Blaizot 2012), cooling from collisional ionization, excitation, recombination, bremsstrahlung, and Compton effect down to 10^4 K. Additional metal-line cooling allows the gas to cool further, down to 0.1 K (Dalgarno & McCray 1972; Sutherland & Dopita 1993).

Star formation is modeled in gas denser than 10 cm^{-3} , with a non-uniform star formation efficiency ϵ_* per free-fall time (Krumholz & McKee 2005; Padoan & Nordlund 2011; Hennebelle & Chabrier 2011; Federrath & Klessen 2012). In short, this model assumes that the unresolved distribution of gas density within a given cell follows a log-normal distribution scaled by the local (resolved) turbulence. The Mach number and virial parameter measured at the scale of the cell then determine which density range of this unresolved distribution should be star forming, using best-fit relations and empirical calibrations from closed-box simulations of the interstellar medium (ISM). This range is then converted into a star formation efficiency for the individual cells, which, once multiplied by an arbitrary scaling factor and divided by the local free-fall time, finally gives the net efficiency ϵ_* (see Dubois et al. 2021; Kraljic et al. 2024, for details). We discuss the implications of this model in Section 5.2.

Feedback from type-II supernovae is modeled by the injection of radial momentum following Kimm & Cen (2014). The simulation also includes the growth and dynamical evolution of massive black holes and their spin (Dubois et al. 2014), and the associated active galactic nucleus (AGN) feedback via the injection of mass, momentum, and energy at low accretion rates (“radio mode”; Dubois et al. 2010), and of thermal energy only at higher rates (“quasar mode”; Teyssier et al. 2011).

Throughout the simulation, galaxies are identified using the clump finder ADAPTAHOP (Aubert et al. 2004) applied to the stellar component. This yields a sample of approximately 150–1400 star-forming galaxies (depending on redshift, with a peak at $z \approx 4$), with stellar masses between $5.7 \times 10^5 M_\odot$ and

¹ <http://new.horizon-simulation.org>

$2.5 \times 10^{11} M_{\odot}$. Thus, our sample does not include analogs of the recently discovered progenitors of extremely massive galaxies undergoing early and rapid evolution (see, e.g., Casey et al. 2024; Carniani et al. 2025). This absence can be explained by either a too small simulation volume not covering the environmental conditions needed to host the formation of such galaxies, and/or missing physical processes, yet to be identified. We refer the reader to Kraljic et al. (2024) for details on the statistical properties of this sample. The mergers events are extracted from the catalogues of Martin et al. (2021), constructed by monitoring the transfert of stellar mass between the progenitor galaxies (Tweed et al. 2009).

2.2. Measurements and robust statistics

Unless otherwise specified, we measure all global quantities within twice the stellar half-mass radius, R_{*} , of each galaxy. Quantities related to star formation activity are computed using stars younger than 10 Myr. The gas fraction is defined as $f_{\text{gas}} = M_{\text{gas}} / (M_{\text{gas}} + M_{*})$, where the total gas mass M_{gas} is measured within $2R_{*}$ and divided by the total baryonic mass in the same volume. To characterize the size of the star-forming gas phase, we compute R_{SF} , the half-mass radius of stars younger than 10 Myr, under the assumption that such stars have not significantly migrated from their formation sites over this short timescale.

All statistical analyses presented below are performed using robust estimators suitable for sparse datasets; that is, we adopt the median instead of the mean, and the robust standard deviation (i.e., the median absolute deviation divided by 0.6745) instead of the classical standard deviation (see Müller 2000; Leys et al. 2013; Romeo et al. 2023, for details). We also use robustly standardized quantities, i.e. quantities centered on the median of their distribution and normalized by their robust standard deviation:

$$X_{\text{std}} = \frac{X - \text{median}\{X\}}{\text{median}(|X - \text{median}\{X\}|) / 0.6745}, \quad (1)$$

which is the robust equivalent of the standardization $(X - \mu) / \sigma$ of a quantity X with mean μ and standard deviation σ .

3. SEMANTICS AND STAR FORMATION REGIMES

Semantical shortcuts and approximations often made in this field can lead to confusion, misinterpretations, and mistakes. To limit this risk, we list here the definitions adopted throughout the paper, and discuss important subtleties.

By construction, the star formation rate (SFR) combines information on the stellar mass produced and the timescale of production. Therefore, a given SFR can equally represent slow but abundant star formation, or rapid but scarce production. To lift this degeneracy and to characterize the underlying physical processes, one can normalize the SFR by either the stellar mass of the galaxy (M_{*}), giving the *specific star formation rate*: $\text{sSFR} = \text{SFR} / M_{*}$, or by the mass of fuel for star formation (M_{gas}), giving the *depletion time*²: $\tau_{\text{dep}} = M_{\text{gas}} / \text{SFR}$. From this, we classify galaxies, as illustrated in Figure 1:

² The inverse of the depletion time is sometimes referred to as star formation efficiency (SFE). This terminology is problematic because this quantity is not an efficiency (which should be dimensionless) and can be confused with the ratio of stellar mass to gas mass — a true efficiency commonly used at the scale of star-forming clouds. These are

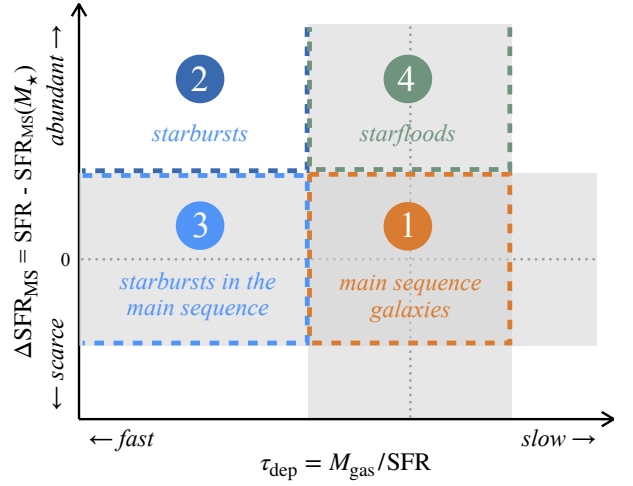


Fig. 1. Schematic classification of star-forming galaxies based on their timescale of star formation (traced by the depletion time τ_{dep}) and their offset from the main sequence ($\Delta\text{SFR}_{\text{MS}}$, i.e., the difference between their SFR and the SFR of the main sequence for their stellar mass). The vertical dotted line represents the median depletion time, and the horizontal one is $\Delta\text{SFR}_{\text{MS}} = 0$. Shaded areas indicate ± 1 times the standard deviation. We highlight four classes and propose an analogy with rivers: the width of the river is $\Delta\text{SFR}_{\text{MS}}$, and the speed of the runoff corresponds to the depletion time. A class-1 galaxy (hereafter a main sequence galaxy) has an average SFR for both its stellar and gas masses, analogous to an average river flow. A class-2 galaxy (hereafter a starburst) forms large amounts of stars at an accelerated pace, analogous to rapid and wide waterfalls. As visible in this diagram, the continuous evolution of $\Delta\text{SFR}_{\text{MS}}$ and τ_{dep} imposes that a galaxy cannot experience a direct transition between classes 1 and 2: it must necessarily pass through classes 3 or 4. Class 3 includes galaxies with rapid star formation but producing average amounts of stars, similar to a tall but narrow waterfall. This work aims to understand the origins of these “starbursts in the main sequence” galaxies (SBMSs). Finally, class-4 galaxies produce large amounts of stars but at a normal rate, analogous to floods. We thus introduce the term “starflood” to name them.

- *Main sequence* is the group of galaxies for which the SFR is close to the median of all galaxies of the same stellar mass at the same redshift. The main sequence is an empirical concept that exhibits redshift- and mass-dependences (see Daddi et al. 2022, for a connection between the bending mass and the cold-to-hot accretion transition mass). It is defined as a best-fit relation in the M_{*} –SFR plane (the form of which remains debated; see, e.g., Speagle et al. 2014; Schreiber et al. 2015; Popesso et al. 2023). Here, we consider as members of the main sequence the galaxies with an SFR within $\pm 1\sigma$ of the best linear fit of the $\log(M_{*}) - \log(\text{SFR})$ relation (which defines $\Delta\text{SFR}_{\text{MS}} = 0$), derived from all star-forming galaxies at a given redshift. The simulation does not probe the massive end of the stellar mass distribution where the observed main sequence yields an inflection (Noeske et al. 2007), and we discuss this important limitation in Section 5.1. Therefore, the functional form we use in the fit to define the main sequence is a simple power-law of the stellar mass, as illustrated in Figure 2. The definition of the main sequence changes as galaxies evolve, and thus we re-compute it at every redshift. For convenience, we use hereafter the term “main sequence” to refer to galaxies of class 1 only

distinct quantities with no clear or systematic link between the two. To stop a long-lasting and misleading confusion, we urge the community not to use the terms efficiency or SFE in place of the inverse of the depletion time.

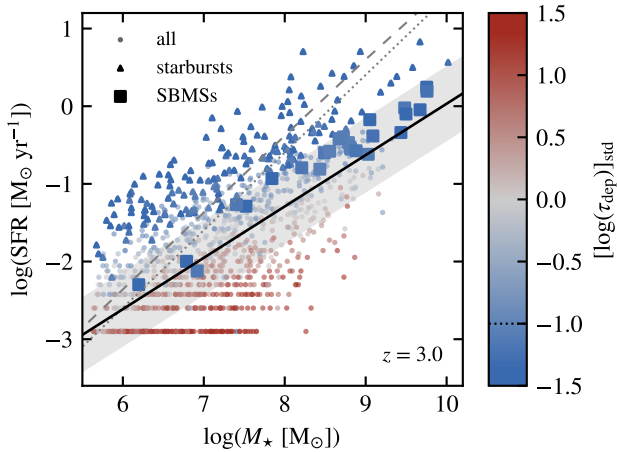


Fig. 2. Distribution of galaxies in the stellar mass–SFR plane at $z = 3$ (for illustration). The color indicates the standardized depletion time (i.e., the difference from the median value of the entire population, divided by the robust standard deviation; see Equation 1). The solid line represents the best least absolute deviation fit, and the shaded area indicates ± 1 times the mean absolute deviation from this relation, defining the main sequence of the simulation at this redshift. For comparison, the dotted and dashed lines show the empirical main sequence relations from fits of observed galaxy populations in Schreiber et al. (2015, their Eq. 9) and Popesso et al. (2023, their Eq. 14), respectively (see Dubois et al. 2021 for a discussion on the main sequence in NEWHORIZON). The horizontal features at low SFR originate from the finite mass resolution of the simulation.

(see Figure 1), separating the galaxies with a short depletion time (class 3, discussed below).

- *Starbursts* are galaxies with a short depletion time. In this work, a galaxy is considered a starburst if its standardized depletion time is below minus unity. In other words, a starburst galaxy forms its stars significantly faster than most other galaxies at the same epoch, regardless of the amount of stars formed. Other works use the term starburst to describe sudden and short-lived increases in the SFR, which is fundamentally different from our definition. Following Renaud et al. (2022), we argue that a definition like ours, based on the timescale of star formation, better reflects changes in the physical regime of star formation, while a definition based on the shape of the SFH could also encompass variations in the availability of star-forming gas without necessarily implying a shift in the mechanisms triggering and/or regulating star formation. Again, for convenience and in agreement with common practice, the term “starburst” refers below to class-2 galaxies only (see Figure 1), and excludes the class 3 made of galaxies with low $\Delta\text{SFR}_{\text{MS}}$.
- *Starbursts in the main sequence* (SBMSs) are galaxies fulfilling the criteria of an unusually short depletion time ($\tau_{\text{dep, std}} < -1$) and being close to the main sequence ($\Delta\text{SFR}_{\text{MS}} = 0 \pm 1\sigma$). While these two conditions could seem mutually exclusive at first sight, it is important to note that the depletion time connects the star formation activity (SFR) with its fuel (gas mass), while the main sequence (and the sSFR) relates the SFR to the stellar mass, i.e., the cumulative history of star formation modulated by accretion and stellar mass loss through feedback. Therefore, the depletion time and the offset from the main sequence are fundamentally independent quantities. A galaxy can theoretically be an outlier according to one criterion while being close to the

average for the other. In this work, we examine which physical conditions and stages of galaxy evolution lead to such situations. As shown in Figures 2 and 3 (made at $z = 3$ for illustration purposes), SBMS galaxies tend to lie on the upper half of the main sequence and can be found over a wide mass range. However, they are preferentially found toward the high-mass end of the distribution at lower redshifts, as these galaxies acquire their stellar mass faster than most others (see Section 4.2 for more details).

- *Starfloods* are galaxies above the main sequence (i.e., with $\Delta\text{SFR}_{\text{MS}} > 1\sigma$) and with a near-median depletion time. As such, their star formation activity is abundant but not particularly fast, hence the analogy with floods. We suspect that such galaxies are rare and/or spend a very short time in this phase during their evolution. We will examine the physics of this regime in a forthcoming paper.

In the following, for convenience, the four classes (main sequence, starbursts, SBMSs, and starfloods) are mutually exclusive. We refrain from adopting observationally-derived definitions of the main sequence and the median depletion time, but rather consider the modeled population of galaxies to build consistent definitions.

In addition, we define the *analogues* as main sequence galaxies with the most similar stellar mass and SFR as the SBMSs: for each SBMS, we identify the nearest³ point that is a main sequence galaxy in the plane of Figure 2. The analogues can then be used as a reference sample in our analysis. Figure 3 shows the distribution of the galaxies studied at $z = 3$ in planes of depletion time, stellar mass, and specific star formation rate. The fundamental difference between τ_{dep} and sSFR noted above explains why these two quantities only very weakly anti-correlate over the entire population, and do not yield any particular relation in the special cases of SBMSs.

Renaud et al. (2022) highlighted the complex, non-trivial and non-monotonous nature of the relation between the position with respect to the main sequence (via $\Delta\text{SFR}_{\text{MS}}$ or the sSFR) and the depletion time, calling for a deeper analysis as we propose below.

4. RESULTS

4.1. First clues on the nature of the SBMS regime from population statistics

We first adopt a statistical approach by monitoring the evolution across cosmic time of the median of key quantities over the entire galaxy populations. This method provides useful indications on the general properties of different families of galaxies. However, these statistics are not representative of individual cases, and thus the connection between such measurements and the underlying physics of galaxy evolution is not direct.

Figure 4 shows that the fraction of star-forming galaxies that have experienced at least one SBMS episode in their lifetime is a linear function of redshift: $-0.10z + 0.68$: after cosmic noon, the majority of star-forming galaxies have been through the SBMS regime at least once. Although this best-fit relation predicts the onset of SBMS galaxies at $z \approx 6.5$, the earliest occurrence in our sample is found at $z = 5.9$. This is, by construction, subject to low-number statistical effects.

³ Since the two axes of Figure 2 do not share the same dimension, it is not possible to rigorously define an unbiased distance metric in this plane. We nevertheless use a definition based on the coordinate system and units of Figure 2 to facilitate our interpretations.

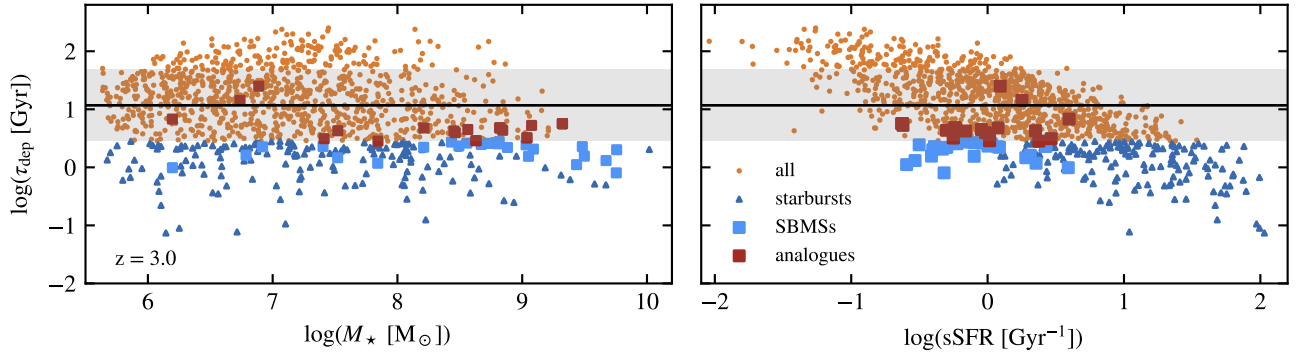


Fig. 3. Depletion times of the total gas of star-forming galaxies as a function of stellar mass (left) and sSFR (right), shown here at $z = 3$. The horizontal line and shaded area show the median τ_{dep} and its dispersion at this redshift. Not surprisingly, the SBMSs are found toward the lower end of the distribution of sSFR of galaxies with short depletion times. This is not a systematic feature since the main sequence is not defined using the M_* –SFR plane.

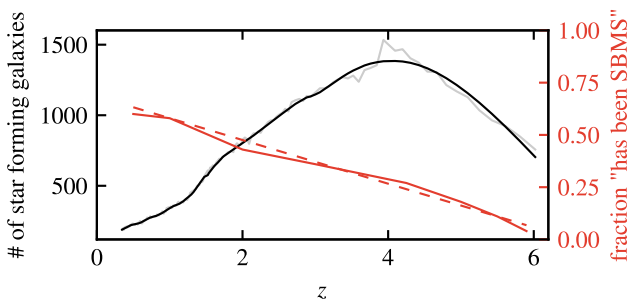


Fig. 4. Number of star-forming galaxies considered in our sample as a function of redshift (grey line and its smoothed version in black, left axis), and fraction of these galaxies that have experienced at least one passage in the SBMS regime in their lifetime (red solid line, and linear fit in dashed red, right axis).

The top panel of Figure 5 reveals that the SBMSs and their analogues are almost always (on average) more massive than the main sequence and starburst galaxies. However, the size of the star-forming gas component (second panel) is significantly smaller in SBMSs than in galaxies with similar SFR and stellar mass. This could be explained by a precocious assembly of the stellar mass of the SBMS galaxies, followed by a slowing down of their star formation activity, possibly due to a dilution of the gaseous phase (see Section 4.3). It may thus be possible –but not inevitable– that SBMS were previously starburst galaxies which have returned to the main sequence, as examined in Section 4.2. At all redshifts, the SBMSs have a significantly lower gas fraction (third panel) than any other class –as expected, on average, from the tightness of the main sequence– and supporting the hypothesis of an overly massive stellar component.

The penultimate panel of Figure 5 shows that the evolution of the number fraction of star-forming galaxies in the starburst and SBMS classes is mild (between 9 and 15% for starbursts, and between 3 and 6% for the SBMSs). This panel also shows that the fraction of SBMS galaxies among the population of galaxies with short depletion times (starbursts and SBMSs) remains approximately constant at 13–18% until $z \approx 2.5$, and increases to $\gtrsim 30\%$ for $z \lesssim 2$. Therefore, the physical conditions necessary for a galaxy to become SBMS change only mildly across cosmic time, at least not monotonically.

Finally, the bottom panel of Figure 5 shows that the median depletion time of the SBMSs is ≈ 1.4 times longer than that of starbursts, with no significant variation with redshift. This difference suggests that SBMSs host different physical conditions from the off-main-sequence starbursts. Thus, SBMSs are not simply the high stellar mass end of the distribution of starburst galaxies, which would naturally explain their lower sSFR, but are rather in a different physical regime, or even at a different stage of their evolution. Conversely, the depletion time of the analogues is ≈ 0.5 times shorter than that of the main sequence galaxies, and the SBMSs exhibit depletion times at least twice as short as their analogues.

Several scenarios proposed to explain the SBMS regime invoke a compaction event in the form of a rapid shrinking of the size of the star-forming material. To test this hypothesis, Figure 6 displays the size ratio of the star-forming to stellar components. The absence of a clear separation of the SBMSs from the other galaxies indicates that their star-forming material does not experience a significant change in size *with respect to the stellar component*. However, Figure 7 reveals that, on average and at all redshifts, the majority of the SBMSs have a stellar component more compact than that in the main sequence galaxies and also in the starbursts (but only a few percent more compact than their non-starbursting analogues). Thus, the compact nature of these galaxies concerns both the stellar and dense gas components, implying a dynamical origin (e.g., tidal stripping of the outer galaxy, loss of angular momentum from tidal torques) but rejecting the possibility of a hydrodynamical-only process which would only affect the gas component (e.g., loss of momentum through shocks or ram pressure). Other configurations might be possible when considering denser environments like that of galaxy clusters, which are not probed in the volume of the NEWHORIZON simulation.

This contradicts one of the interpretations of Magnelli et al. (2023) and Lyu et al. (2025), who, using the CEERS survey (JWST/MIRI), identify galaxies with a compact star-forming component embedded within an extended stellar disk (their “EC” class) and tentatively associate them with SBMS. In their scenario, the EC/SBMS event is triggered by the compaction of the dense gas, increasing the central star formation density, and driving the in-situ build-up of a bulge-like morphology (see also Le Bail et al. 2024; Tan et al. 2024 reporting centrally luminous infrared galaxies with extended stellar disks). In our simulation, such an evolution also triggers an elevation of the star forma-

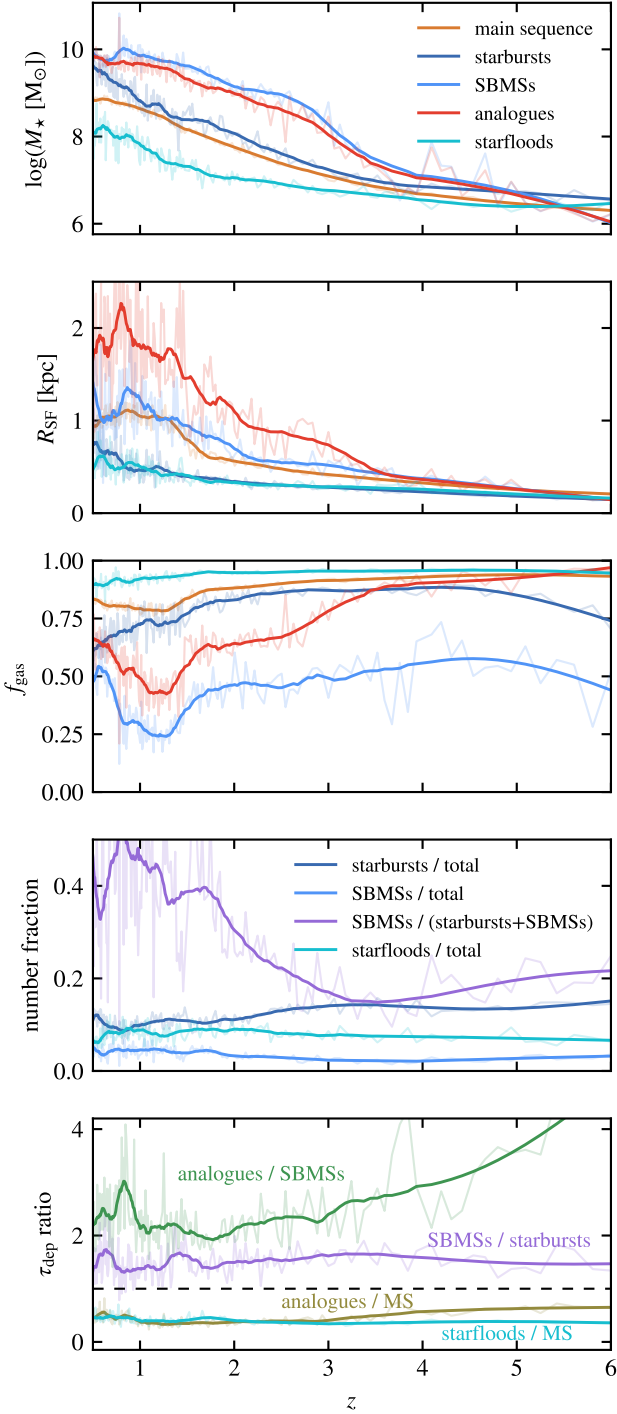


Fig. 5. *Top three panels:* evolution of the median of the logarithmic stellar mass, the half-mass radius of the star-forming gas, and the gas fraction for galaxies in the main sequence, in the starburst regime, in the SBMS regime and their analogues (i.e., the non-starburst main sequence galaxy with the most similar SFR and M_\star), and in the starfleet regime (see Section 3 for details). *Penultimate panel:* evolution of the number fractions of each regime over the entire population of star-forming galaxies. Also shown is the fraction of SBMSs among galaxies with short depletion times (i.e., starbursts and SBMSs). *Bottom panel:* median depletion time of the SBMSs normalized by that of the starburst galaxies, and the same ratio between the analogues and the main sequence galaxies, and between the analogues and the SBMSs. The horizontal line indicates unity. All curves have been smoothed using a Savitzky–Golay algorithm to improve readability, with the original measurements shown by the semi-transparent lines.

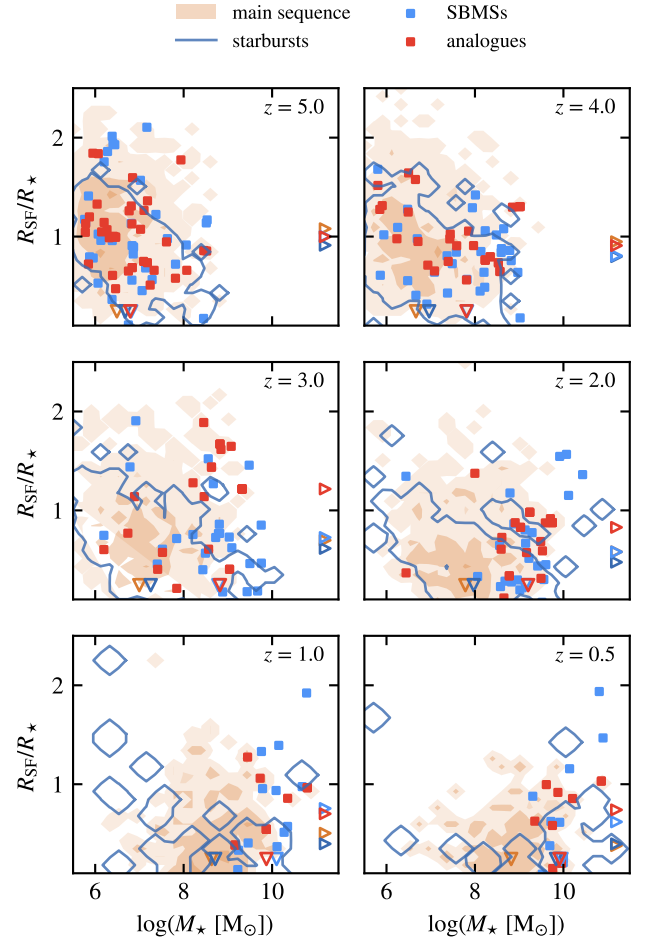


Fig. 6. Ratio of the size of the star-forming (R_{SF}) to the stellar component of galaxies, as a function of stellar mass, for all star-forming galaxies at six different redshifts. R_{SF} is computed as the half-mass radius of the stars younger than 10 Myr, and is used as a proxy for the size of the star-forming gas phase. Filled contours indicate the distribution of the main sequence galaxies, and that of the starbursts is shown by the solid line contour. The SBMSs and their analogues are shown as squares. Triangles on the right and bottom axes indicate the median values of both quantities for each population. For $z \gtrsim 2.0$, SBMS galaxies are found across the mass and size ranges of the star-forming galaxies and are only confined to the high-mass end at later epochs. Apart from this, the distributions of SBMS galaxies in this plane are not very different from those of the other classes, which contradicts scenarios in which a compaction event marks the onset of the SBMS regime.

tion rate, but not a drop in depletion time, and thus cannot be associated with the SBMS regime (see Figure 12 for details). The discrepancy originates from the different definitions used to identify starbursts. While we base our criterion on physical quantities, such measurements are notoriously more challenging in observations. The gas mass is often unavailable, or at best subject to important uncertainties and the necessity to assume standard scaling relations to derive it (e.g., Accard et al. 2025). As a result, the observed galaxies are rarely classified according to their depletion time but by the compact nature of their star-forming component (as in Magnelli et al. 2023; Lyu et al. 2025), which blurs or skews their identification as starbursts or SBMSs.

Our results are also in tension with the scenario of Puglisi et al. (2021), who propose that SBMSs result from merger-driven nuclear gas inflows leading to starburst activity, followed by a

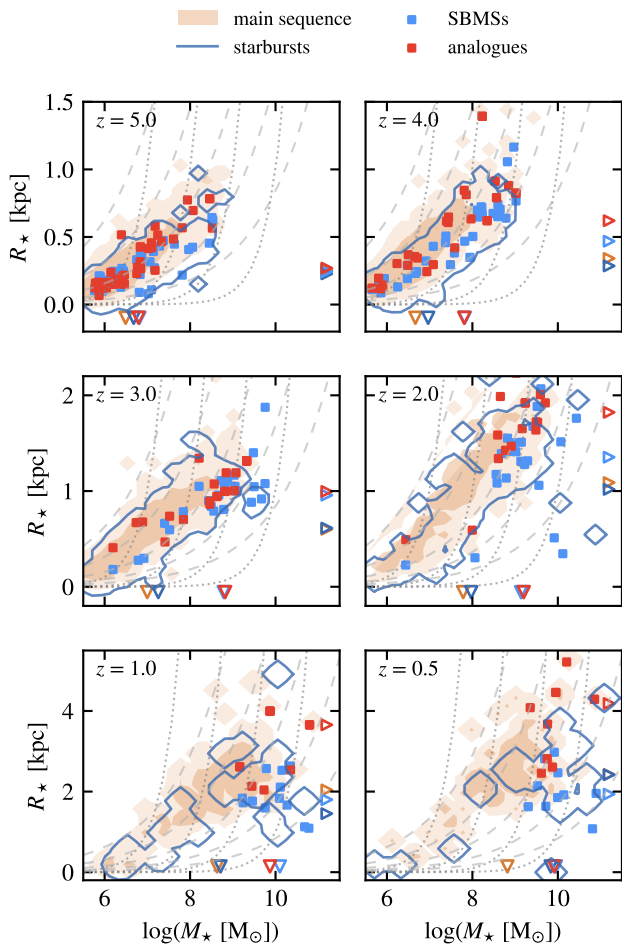


Fig. 7. Same as Figure 6 but showing the stellar mass–size relation. Dotted (respectively dashed) guiding lines indicate constant compactness ($M_* \propto R_*^3$) and constant density ($M_* \propto R_*^3$), spaced by factors of 10 and 2, respectively. The range of the vertical axis changes between the rows for readability, but the guiding lines remain identical in all panels. On average, the SBMSs are more compact than galaxies from the other classes.

post-merger evolution through the main sequence and toward quenching (e.g., Barro et al. 2014; Puglisi et al. 2019), but maintaining an extended stellar component (see also Elbaz et al. 2018; Franco et al. 2020; Tadaki et al. 2020). During a merger, tidal torques affect all components (Mihos & Hernquist 1996) and thus, purely gaseous inflows could only be caused by another mechanism as discussed in Tan et al. 2024 to explain the in-situ build-up of bulge-like structures in submillimeter galaxies.

The picture emerging from our analysis so far is that of an early and rapid assembly of the stellar component favoring a low sSFR to explain the properties of the SBMSs. We stress that this rapid assembly does not necessarily immediately precede the SBMS episode (see Section 4.3 for an analysis of the short-term evolution of individual galaxies before and after the SBMS phase). Contrary to interpretations from the literature, we do not detect in SBMSs any significant recent compaction of the gas reservoir in an extended stellar component (i.e., SBMSs, whose starburst nature is defined by depletion time rather than a compact infrared component, are not necessarily associated with the EC galaxies of Lyu et al. 2025) but rather both stellar and gaseous components being more compact than average (the CC

class of Lyu et al. 2025). We discuss in Section 4.3 whether the compactness is a fundamental trigger of the SBMS regime. Furthermore, the peculiarities of the SBMSs do not seem to vary with redshift.

We cannot yet conclude on the role of punctual events such as mergers, as their impacts are not synchronized over the full population of galaxies and are thus smoothed out in statistical analyses. Two examples of the full history of SBMS galaxies at $z = 3$ are shown in Appendix A to illustrate the complex and non-monotonic evolution of galaxies above, within, and below the main sequence. All cases we examined yield similar highly-time-varying, stochastic, evolutions (see also Gui et al. 2025). This contradicts a number of proposed scenarios in which the SBMS phase is a mere transition between a starburst phase and definitive quenching (e.g. Tacchella et al. 2016; Puglisi et al. 2019). We stress again that the fluctuations noted in these examples are smoothed out when computing statistical quantities over a large number of galaxies (e.g., the main sequence), demonstrating that statistics are not representative of individual histories, and thus cannot probe full complexity of the underlying physical processes.

4.2. Early history of SBMS galaxies: the role of mergers

The results of the previous section suggest that at least part of the peculiarities of SBMS galaxies originates in a precocious assembly of their stellar component, from external (accretion of companion galaxies) and/or in situ origins (star formation). To explore this further, we compare the histories of SBMSs with those of the other classes of galaxies. To ease interpretation, we focus at $z \approx 3$ as a compromise between an epoch late enough to cover a diversity of galactic morphologies and histories (see Dubois et al. 2021; Kraljic et al. 2024) and still early enough to keep their histories simple. We generalize our conclusions to other redshifts in Section 4.4. The galaxies are classified at $z = 3$ according to the definitions in Section 3, and then tracked back in time by identifying their most massive progenitor on each previous snapshot, i.e., every $\approx 10 - 15$ Myr.

Figure 8 reveals that the median number of major mergers in the history of SBMS galaxies is 1.5 times higher than for the starbursts and the analogues. Despite SBMSs being preferentially found among the most massive galaxies (which implies most of their encounters happen with lower-mass galaxies), they experience significantly higher numbers of both minor and major mergers than the starburst galaxies, and more major mergers than their analogues. Therefore, the increased stellar mass of SBMSs is caused, in part, by repeated merger events.

In addition to accretion of neighbor galaxies, in situ star formation is the only other pathway to grow the stellar component. Rapid star formation is often associated with wet major mergers which can trigger nuclear inflows, shocks, and tidal and turbulent compression. Experiencing many major mergers is thus compatible with a precocious growth of the stellar mass from both in situ and external origins. However, the response of galaxies to the stimulus of a major merger in terms of star formation is not constant across cosmic time as it depends on the morphology (Segovia Otero et al. 2022) and gas fraction of the progenitor galaxies (Perret et al. 2014; Fensch et al. 2017), and possibly on other factors too. Although examining each merger event individually is beyond the scope of this paper, Figure 9 shows that the SBMSs and their analogues have spent respectively 3.5 and 4 times more time in the starburst regime than the main sequence

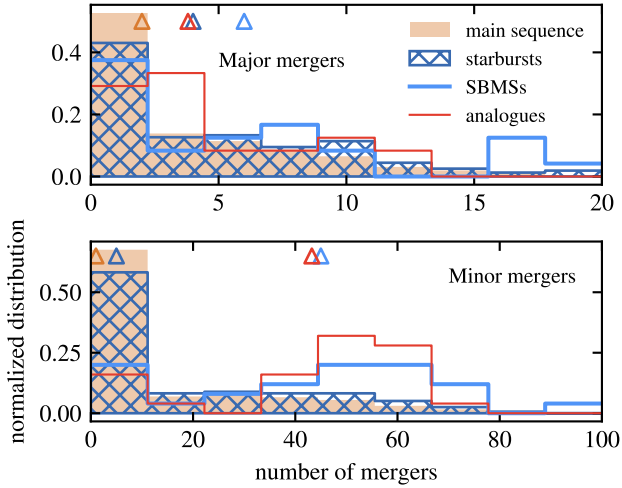


Fig. 8. Normalized distributions of the number of major (top, mass ratio $> 1:10$) and minor mergers (bottom, mass ratio between $1:10$ and $1:50$) experienced by galaxies identified and classified at $z = 3$. The triangles indicate the median values for each population. Changing the mass-ratio thresholds for the definitions of major and minor mergers alters these distributions but not our conclusions. SBMS galaxies experience more major and minor merger events than the other classes, which contributes to the early build-up of their stellar mass by accretion and merger-triggered starbursts (see also Figures 9 and 10).

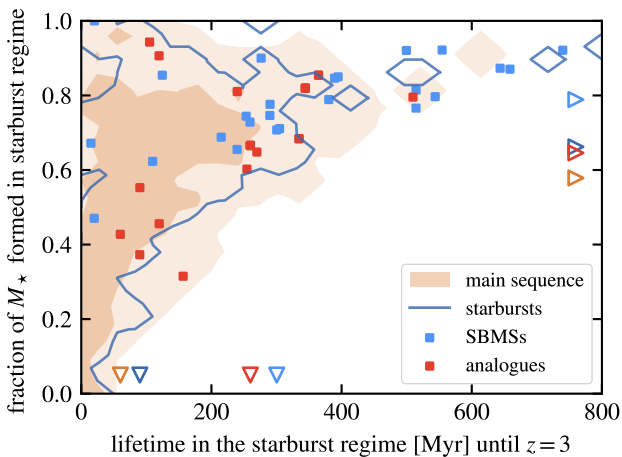


Fig. 9. Importance of the starburst regime in the history of the galaxies found at $z = 3$, shown by the lifetime they spent as starburst and the fraction of their stellar mass they formed in this regime (irrespective of the number of starburst episodes experienced). The triangles near the bottom and right axes indicate the median values for each population. SBMSs are clearly distinguished by longer and more productive starburst episodes.

and the other starburst galaxies at $z = 3$.⁴ The difference between the SBMSs and their analogues is more pronounced when considering the fraction of stellar mass formed during these starburst episodes: SBMSs stand out by a production of stars 20% faster than the other galaxies including their analogues, that is, a short depletion time during the starburst episodes they experienced, as confirmed in Figure 10. When considering their entire

⁴ With the cosmological parameters assumed in NEWHORIZON, the age of the Universe is ≈ 2200 Myr at $z = 3$.

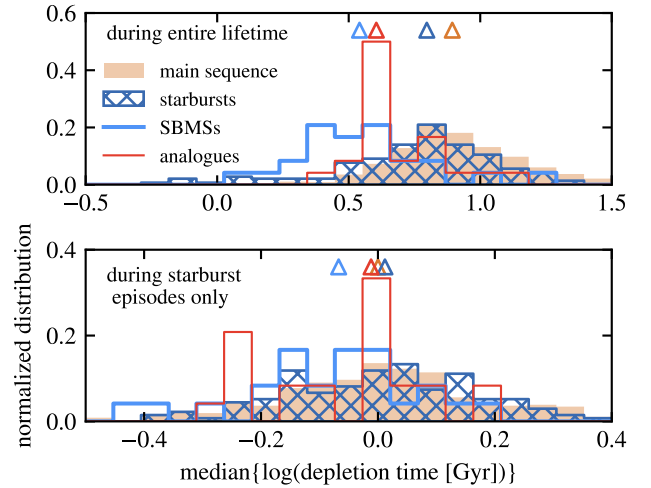


Fig. 10. *Top:* Normalized distributions of the median logarithmic depletion time of galaxies between their formation and their classification at $z = 3$. *Bottom:* same but considering only the depletion times during the starburst episodes. Triangles indicate the median of the distributions.

lifetime (top panel of Figure 10), SBMSs and their analogues have similar median depletion times, about 1.6 times shorter than the starbursts and main sequence galaxies. However, the distribution of SBMSs extends significantly further toward short depletion times, and episodes of long depletion times are rarer for SBMS galaxies than for the others. This could potentially be explained solely by the differences in number of major mergers (Figure 8), but when selecting only the starburst episodes along the lifetime (bottom panel), the SBMSs appear to host star formation approximately 15% faster than that of all the other galaxies. Furthermore, major mergers of starburst and SBMS galaxies are 1.4 times more frequent than for galaxies with longer depletion times (Figure B.1) and the ratio of major to minor mergers is 1.3 times higher for SBMSs than for their analogues. Owing that interactions with massive galaxies are generally more efficient at triggering starbursts than those involving a smaller companion (Cox et al. 2008; Ellison et al. 2008), mergers that are more numerous, more frequent, and involve more massive companions explain the rapid star formation in SBMSs.

For the events considered here, we find no particular relation between short depletion times and an early settling of the disk (which would be more prone to responding to mergers by triggering starburst events; Segovia Otero et al. 2022), nor with a lower gas fraction than in other galaxies (Perret et al. 2014; Fensch et al. 2017). The underlying physical cause of the merger-triggered starbursts could then possibly be stronger compression generating an excess of dense gas which, in turn, increases the SFR and decreases the depletion time (Renaud et al. 2014). Repetitions of such events enable these galaxies to quickly assemble their stellar component, in addition to the frequent accretion of their companions, which naturally tends to lower their sSFR and $\Delta\text{SFR}_{\text{MS}}$, and make them SBMSs. Renaud et al. (2022, their Figure 3) shows that the compression varies strongly with the large-scale environment, suggesting that SBMSs could lie in specific locations of the cosmic web favoring frequent and starburst-efficient mergers. We will test this hypothesis in a forthcoming paper.

In summary, on average, SBMS galaxies distinguish themselves by precocious and intense starburst activity likely connected to frequent major mergers, during which they assemble

a significant fraction of their stellar component by accretion and merger-triggered rapid star formation. Galaxies from the other classes experience fewer and less frequent mergers, spend less time in starburst mode, and yield longer depletion times during these episodes. The dispersions of the distributions shown in Figures 9, 10, and B.1 suggest that these generalities cover a diversity of finer scenarios, which we examine further in the next section.

4.3. Evolution before, during, and after the SBMS episodes

Figure 1 shows that the SBMS class can be a transition stage between starburst and main sequence, as often supposed in the literature. However, other paths are possible in the $\tau_{\text{dep}} - \Delta\text{SFR}_{\text{MS}}$ plane. In this section, we classify SBMS galaxies according to their class immediately before and immediately after their SBMS episode. Four sub-categories of SBMS⁵ appear according to the chronological sequence of the classes:

- 1-3-2: from main sequence to starburst (“MS to SB”),
- 2-3-2: from starburst to starburst (“SB to SB”),
- 2-3-1: from starburst to main sequence (“SB to MS”),
- 1-3-1: from main sequence to main sequence (“MS to MS”).

To improve the statistics⁶, we stack the SBMS episodes detected on snapshots within ± 250 Myr of $z = 3$. In this time window, the four sub-classes comprise approximately 9%, 39%, 22%, and 30% of the SBMS galaxies, respectively. Therefore, about two-thirds of the galaxies return to their previous regime after the SBMS phase. (These numbers vary with redshift; see Section 4.4.) Among the remaining third, the majority reduces its star formation activity (“SB to MS”). Despite being the most discussed option in the literature (as a possible route toward quenching; see e.g., Puglisi et al. 2021; Gómez-Guijarro et al. 2022), this pathway concerns less than one quarter of the entire SBMS population in NEWHORIZON.

Figure 11 shows that, at $z = 3$, the longest SBMS episodes occur in the most massive galaxies, and most of these massive systems then return to their previous class (“SB to SB” and “MS to MS”). Shorter SBMS episodes occur across all masses and evolutionary types. Rapid in-and-out transitions of the SBMS phase are likely caused by fluctuations of the SFR on comparable timescales (see Figure A.1). Lower-mass galaxies, being more responsive to rapidly changing internal and environmental regulators of star formation (feedback, compaction, mergers; Dekel & Burkert 2014; Muratov et al. 2015; Christensen et al. 2016), naturally experience the shortest SBMS episodes. Galaxies that transition from one regime to another (“MS to SB” or “SB to MS”) spend the least time as SBMS. The limited output cadence of the simulation (of order 15 Myr at this epoch) likely influences these measurements: the shortest SBMS episodes may be unresolved.

The bottom panel of Figure 11 confirms the peculiarity of SBMSs and their sub-classes in terms of gas fraction. Overall, the gas fraction of our star-forming galaxies decreases monotonically with increasing stellar mass. Regardless of mass, SBMSs

⁵ The transition of SBMS galaxies to/from galaxies with short depletion times and low $\Delta\text{SFR}_{\text{MS}}$ (i.e., “starbursts below the main sequence”) is not detected in the simulation.

⁶ Cases for which the phase immediately preceding and/or succeeding the SBMS episode lasts less than two consecutive snapshots are ignored. This removes the SBMSs and analogues of the lowest mass ($\lesssim 10^7 M_{\odot}$) from the sample considered in this section, as the extreme stochasticity of their star formation properties challenges a robust identification of their evolutionary path through the SBMS phase.

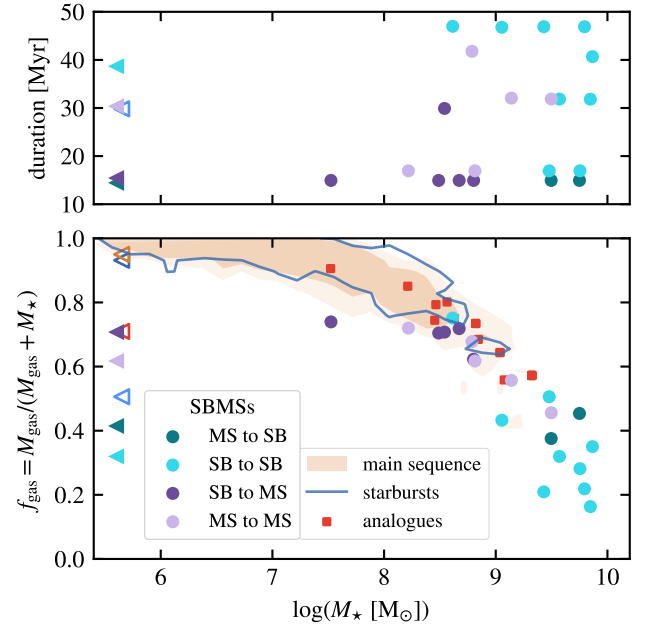


Fig. 11. Duration of the current SBMS episode (*top*) and gas fraction (*bottom*) for the SBMS galaxies detected at $z = 3$, shown as a function of stellar mass. The SBMS galaxies are classified according to their trajectory in the $\tau_{\text{dep}} - \Delta\text{SFR}_{\text{MS}}$ plane before and after the SBMS phase (see text). The triangles to the left of the panels indicate the median value of each group (with all SBMSs in light blue). In the top panel, a small vertical offset has been added to the “SB to SB” and “MS to MS” points to avoid graphical overlap with other points; this offset is not used when computing the medians.

lie at the lower end of the gas-fraction distribution. These low f_{gas} mainly result from a high stellar mass (which we also invoke to explain their low sSFR and low $\Delta\text{SFR}_{\text{MS}}$, recall Section 4.1) rather than small amounts of gas. Therefore, even with low f_{gas} , SBMSs are potentially capable of re-igniting a starburst activity. Indeed, the most massive SBMSs—those with the lowest gas fractions—are galaxies on the verge of becoming starbursts within, at most, a few 10 Myr (as noted above). At slightly lower masses—and thus significantly higher gas fractions—lie SBMSs that will next become main sequence galaxies. Therefore, the short-term future evolution of SBMSs is related to the gas fraction. Conversely, their recent past does not correlate with either gas fraction or stellar mass, since these quantities result from the assembly of the gas and stellar components over long timescales.

Several scenarios propose to connect SBMSs to a compaction episode that would trigger starburst activity in turn leading to the exhaustion of the star-forming gas (e.g., Gómez-Guijarro et al. 2022). However, the link between kpc-scale accumulation of gas and the pc-scale change of gas density that sets the star formation activity is not yet fully understood. In particular, while a compaction event is commonly expected to increase the SFR by raising the amount of dense gas, it is not clear whether this necessarily implies a decrease in depletion time (Lapiner et al. 2023). In any case, our analysis does not confirm a dominant role of compaction in the SBMS phase (recall also Figure 6), but the statistical nature of the results shown in Section 4.1 leaves open the possibility that this scenario only concerns a specific evolutionary pattern limited to a sub-category of SBMSs, as we test below.

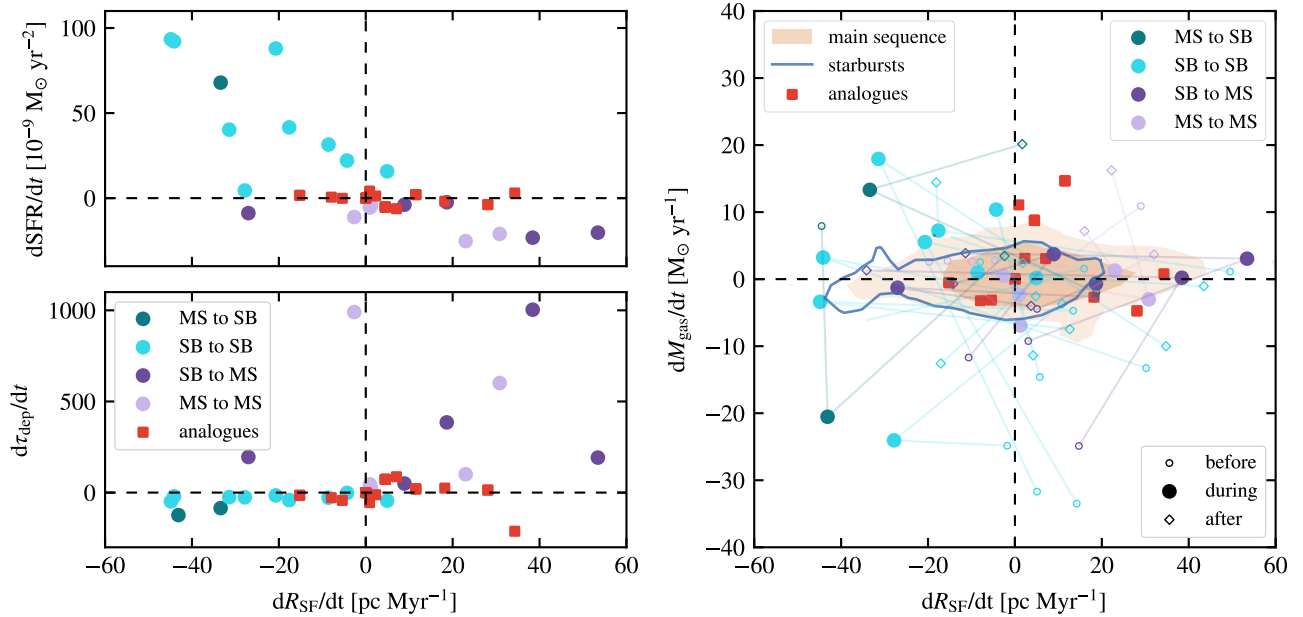


Fig. 12. Variations of the star formation rate (*top-left*), of the depletion time (*bottom-left*), and of the gas mass within twice the half-mass stellar radius (*right*), compared to the change in half-mass radius of the star-forming gas (traced by stars younger than 10 Myr) at $z = 3$. All variations are measured over the exact duration of each galaxy’s SBMS episode, or over 30 Myr for the non-SBMS galaxies shown for reference (i.e., similar to the median duration of an SBMS episode; recall Figure 11). SBMSs are color-coded according to the sub-class they belong to before and after the SBMS phase (see text). The main sequence and starburst galaxies are omitted in the left panels for clarity. In the right panel, for each SBMS galaxy, lines connect the measurement during the SBMS episode to measurements 30 Myr immediately before (empty circles) and after (empty diamonds) the episode, indicating a three-point evolutionary track in this plane.

The left panels of Figure 12 compare variations in the size of the star-forming ISM (traced by the half-mass radius of stars younger than 10 Myr) to changes in SFR and depletion time over the entire SBMS episode, and over 30 Myr for the analogue galaxies shown for reference. These analogue galaxies maintain their SFRs and depletion times despite non-negligible compaction or dilation of their star-forming ISM (up to kpc scales during the period considered). This strikingly contrasts with the SBMS galaxies, which show unambiguous responses to size variations. Moreover, a clear dichotomy appears in this figure between SBMSs that become starbursts and those that become main sequence galaxies.

SBMSs that will become starbursts (“MS to SB” and “SB to SB”) experience a compaction of their star-forming ISM ($dR_{\text{SF}}/dt < 0$). This translates into an increase of the SFR (approximately as $d\text{SFR}/dt \propto -1.5 M_{\odot} \text{ kpc}^{-1} \text{ yr}^{-1} \times dR_{\text{SF}}/dt$), but only into a very weak acceleration of the star formation process. Indeed, the variations in τ_{dep} for these galaxies are of the same order as those in the analogue reference sample, and thus not related to the SBMS physics. Conversely, SBMSs on their way to become main sequence galaxies (“SB to MS” and “MS to MS”) experience a dilation of their star-forming ISM during the SBMS episode ($dR_{\text{SF}}/dt > 0$), which induces a mild diminution of the SFR (yet significantly more pronounced than the variations in the analogue sample). Given the moderate change in gas mass for these galaxies (visible in the right panel of Figure 12), this necessarily leads to a lengthening of the depletion time, as confirmed in the bottom-left panel (approximately $d\tau_{\text{dep}}/dt \propto 4.2 \text{ Myr } M_{\odot} \text{ pc}^{-1} \times dR_{\text{SF}}/dt$, but with an important scatter). Such dilation events are thus directly connected to the change of star formation regime from starburst (abundant and fast) to main sequence (scarcer and slower). If caused by

feedback, the absence of significant mass-loss indicates a redistribution of the gas within the galaxy instead of outflows, or a balance by accretion at the same rate.

The right panel of Figure 12 also shows the evolution of galaxies shortly before, during, and shortly after their SBMS phase at $z = 3$. The variety of tracks contrasts with the simplicity of statistical trends described above: while SBMS galaxies appear as systems that precociously assemble their stellar mass (Section 4.2), their evolution over short-timescales ($\sim 30\text{--}100$ Myr) is far from universal. Nevertheless, all tracks reach an extremum in either mass- or size-growth rate (or both) during the SBMS phase, confirming the peculiar and transitional character of this phase along galaxy evolution. It appears that the nature of this extremum and its relation to the preceding and following phases distinguish the SBMS sub-classes.

Starbursts that experience an SBMS phase before returning to the starburst class (“SB to SB”) typically show an initial reduction of gas mass due to accelerated consumption by star formation, accompanied by a mild size growth of the star-forming phase –possibly caused by efficient gas redistribution by stellar feedback. After a compaction during the SBMS phase (often associated with an accumulation of gas), they resume their off-main-sequence starburst activity with a size expansion but with no unique trend in the evolution of their gas mass. This diversity likely reflects the variety of physical processes that trigger starbursts, each with its own timescale that can or cannot overcome the replenishment of the gas reservoir (Renaud et al. 2019a). For the same reason, no clear trend is found for main sequence galaxies that become starbursts (“MS to SB”). In virtually all cases, galaxies that become starbursts after the SBMS phase experience the strongest compaction of their star-forming ISM during the SBMS phase, along the scenario of formation of blue nuggets

(Dekel & Burkert 2014). However, because the SBMS phase is short-lived (Figure 11), these galaxies do not have enough time to exhaust their gas reservoir and do not become red nuggets. Therefore, compaction leading to a SBMS phase is not a direct pathway toward a quiescent or quenched galaxy, but rather toward the (re-)ignition of a starburst activity.

Main sequence galaxies that temporarily become SBMSs (“MS to MS”) do not experience statistically significant changes in gas mass or size: their distributions in the right panel of Figure 12 are concentrated around the no-growth position, similar to the non-SBMS galaxies. The brief passage through the SBMS phase for these systems could be caused by rapid fluctuations in the conditions for star formation. More generally, the gas mass of SBMS galaxies that move toward the main sequence (“MS to MS” and “SB to MS”) does not change significantly during the SBMS episode, but tends to increase slightly afterward. This could possibly result from an imbalance between steady gas inflows from large scales and a slowed consumption by star formation. Thus, whether an SBMS progenitor was a starburst or a main sequence member, an SBMS episode does not mark a step toward quenching.

The evolutionary path from starburst to quiescent galaxy via the SBMS regime, as proposed by Puglisi et al. (2021) in the context of quenching, concerns at most a quarter of our simulated sample, and this fraction is even lower at other redshifts, see Section 4.4. Our measurements rather support scenarios where the SBMS is a short-lived step along a diversity of evolutions, better compatible with the first steps in the proposition of Gómez-Guijarro et al. (2022), namely repeated passages in and out of the main sequence, before quenching (see also Lyu et al. 2025). Although most of the results we present above are robust to changes of numerical methods and initial conditions, we discuss possible sensitivities of our conclusions to these aspects, notably the galactic mass, in Section 5.

4.4. Generalization to other redshifts

The conclusions above have been obtained from the analysis of the galaxy population at $z = 3$. Generalizing to higher redshifts suffers from low-number statistics, while at later epochs, galaxies experience increasingly complex formation histories, possibly complicating the interpretations proposed above. Nevertheless, both the cosmological environment (e.g., the merger rate) and the intrinsic evolution of galaxies require assessing the validity range of our conclusions. We describe here the main differences between our conclusions at $z = 3$ and results from the same protocol conducted at other redshifts⁷.

The most prominent evolution with redshift is the progressive depletion of SBMS galaxies toward the low-mass end of the galaxy mass function at low redshift (visible in, e.g., Figure 6). This naturally derives from the early assembly of the stellar component via accretion and enhanced in situ star formation, which is central to our scenario.

At high redshift ($z \gtrsim 4$), despite lower number statistics, virtually all the quantities examined yield smaller scatters. This is caused by galaxies having had less time to significantly diverge from a relatively uniform evolutionary pathway, i.e., the diversity of histories is not yet fully developed. Considering a larger cosmological volume (e.g., including galaxy protoclusters) would likely mitigate this conclusion.

⁷ As before, the main sequence and median quantities are re-computed and the galaxies are re-classified at each redshift.

Towards low redshifts, the number of mergers experienced by SBMSs increases less than that of any other class: after $z \approx 1$, the other classes yield a higher number of major mergers, and a similar number of minor mergers than SBMSs, on average (see Figure B.3). The frequency of major mergers steadily decreases with time for all classes (Martin et al. 2021), and ceases to be enhanced for SBMSs at $z \lesssim 1$ (Figure B.2).

Although the median duration of the SBMS episodes does not change across cosmic time, short episodes ($\lesssim 20$ Myr) become rarer at low redshifts. This is likely caused by longer dynamical timescales in increasingly more massive galaxies. Notably, the “MS to SB” transition is twice as long at cosmic noon ($z \approx 2$) as at any other redshift (≈ 40 Myr), possibly linked to a longer interaction timescales if this transition is merger-triggered. The fraction of SBMS galaxies returning to their previous class (“SB to SB” and “MS to MS”) increases significantly with decreasing redshift: while these sub-categories are absent at $z \gtrsim 3$, they represent $\approx 70\%$ of the SBMSs at $z \lesssim 2$. The transition from starburst to main sequence (“SB to MS”) is virtually nonexistent at $z \geq 4$ and remains rare at all redshifts (2% at $z = 2$, 10% at $z = 1$), with its maximum reached at $z = 3$ (22%). This further challenges the proposition commonly found in the literature of SBMS being a transition phase between starburst and quiescent galaxies: while possible, this scenario concerns less than a quarter of the SBMS galaxies at any redshift.

The dependences of the variations of SFR, τ_{dep} , and the size of the star-forming component remain the same at all redshifts, with the same differentiation between the sub-categories of SBMS galaxies. We note, however, that variations in τ_{dep} during the SBMS phase are less important at both higher and lower redshifts than at $z = 3$.

In summary, the scenario proposed in the previous sections from our analysis at $z = 3$ remains valid throughout cosmic time. Quantitative variations arise from the overall evolution of the gas contents and merger rate, but follow the general trends of galaxy evolution, irrespective of the SBMS regime. This demonstrates that the SBMS behavior is a recurrent mode of star formation, embedded within the broader evolutionary trends of star-forming galaxies.

5. DISCUSSION

5.1. Extrapolation to more massive galaxies

In the GOODS-ALMA sample, SBMSs are found between $\approx 10^{10.2}$ and $10^{11.5} M_{\odot}$ at $z \approx 1-2$ (Elbaz et al. 2018; Ciesla et al. 2023), that is, approximately an order of magnitude more massive than the average of our modelled cases (Figure 5). The NEWHORIZON simulation has been designed to explicitly avoid dense cosmological environments favoring the assembly of the most massive galaxies, such as galaxy clusters. As a result, the maximum stellar mass in the simulation volume is $M_{\star} \approx 10^{11} M_{\odot}$ at $z = 0$. Since different mechanisms are involved in galaxy evolution across the mass spectrum, the mass discrepancy between the observed and modelled samples could indicate that our scenario for SBMSs might not fully apply to more massive galaxies.

Although the merger rate only weakly scales with stellar mass (Lotz et al. 2011; O’Leary et al. 2021), other mechanisms show a much stronger mass dependence. For example, gas accretion transitions from cold to shock-heated at virial masses of $\approx 10^{12} M_{\odot}$ (Birboim & Dekel 2003). Combined with stronger AGN feedback and shorter depletion times (Fabian 2012; Tacconi et al. 2020), this can result in a slower replenishment of the

gas reservoir after an intense starburst episode (Dekel & Birnboim 2006; Peng et al. 2010). In this case, the SBMS phase would then represent a transition toward quenching, as postulated by Tacchella et al. (2016) and Gómez-Guijarro et al. (2022).

However, our analysis reveals very few and only weak dependencies of our scenario on stellar mass. Therefore, either our conclusions apply across the mass spectrum, or there exists a critical mass (such as the $\approx 10^{12} M_{\odot}$ threshold for the virial mass from Birnboim & Dekel 2003 and proposed by Daddi et al. 2022 as a transition to explain the bending of the main sequence as a function of stellar mass; see also the discussion in Lapiner et al. 2023 on its role on the compaction mechanism) above which our scenario must be adjusted to account for different relative roles of the physical processes governing galaxy evolution. For instance, Puglisi et al. (2019) noted that fraction of main sequence galaxies exhibiting compact star forming regions increases significantly for the most massive cases of their sample ($M_{*} \gtrsim 10^{11} M_{\odot}$). Similar results are reported on the EC class of Lyu et al. (2025, i.e., compact gas in extended stellar component), supporting the idea of a mass-dependence of the compaction-driven evolution of star forming galaxies. The authors interpreted these galaxies as early post-starbursts, therefore possibly connected to the SBMSs (recall Section 4.1).

5.2. Dependence on the sub-grid recipe of star formation

The sub-grid model of star formation implemented in NEWHORIZON assumes that the unresolved gas content of a cell can be described by an empirical model calibrated on closed-box simulations of the ISM (see Dubois et al. 2021). Doing so requires choosing several properties of the unresolved gas, mainly its density distribution and turbulence spectrum. In the model used here, the unresolved density PDF is assumed to be log-normal, with a variance set by the Mach number and with energy equipartition between the solenoidal and compressive modes of turbulence (Federrath & Klessen 2012). The density threshold for star formation in this unresolved medium is set by the product of the Mach number and the virial parameter, computed as the ratio of thermal and turbulent pressures to gas self-gravity. These choices then set the star formation efficiency of each gas cell (denser than a threshold of 10 cm^{-3} , arbitrarily chosen).

By assuming that closed-box ISM models can be directly scaled to represent the unresolved content of a cell in cosmological or galactic simulations, one necessarily underestimates the coupling between these scales. For instance, shear and tides—which generally stabilize the gas—and the external potential from stars and dark matter—which has the opposite effect—are not accounted for in our sub-grid model. Furthermore, the assumption of a log-normal shape with equipartition of turbulent modes for the unresolved density PDF ignores possible variations caused by compression and external forcing of turbulence. Such assumption would then lead to mis-representations of the true, unresolved distribution of gas over timescales depending on the nature of the forcing and the associated decay of turbulence. This is particularly critical in compressive environments (mergers, galactic centers, spiral arms) and also varies with redshift (Renaud et al. 2019a, 2022). The consequence is a minimization of the diversity of turbulence spectra, and thus a tendency toward the homogenization of star formation regimes.

Therefore, the adopted sub-grid recipe may artificially reduce the importance of non-standard star formation regimes, such as starbursts, notably in terms of the intensity of the bursts. Predicting how our quantitative conclusions are affected likely

requires a full understanding of the physics of scale coupling between the simulation resolution (34 pc) and the scale of star formation itself. For instance, the nature of the turbulent cascade from kpc-scale injection to dissipation, and the role of external forcing, remain to be understood. Higher-resolution simulations that capture smaller scales (at the cost of sacrificing simulation volume and thus environmental diversity), as well as observations that (marginally) resolve star-forming regions, report wide ranges for the relevant quantities such as the star formation efficiency per free-fall time, the virial parameter, the Mach number, and the index of the turbulence power spectrum (Renaud et al. 2013; Lee & Hennebelle 2016; Grisdale et al. 2019; Rosolowsky et al. 2021; Segovia Otero et al. 2025).

Acting as a regulator of star formation, stellar feedback is expected to reduce the impact of these artefacts on star formation activity. However, the delay between star formation and feedback can be comparable to the dynamical timescales of star-forming regions, especially in fast-evolving environments such as mergers. The structure and properties of the ISM may then differ significantly between the onset of star formation and its expected regulation. In addition, uncertainties persist regarding the efficiency and scale of feedback coupling with the ISM (Agertz & Kravtsov 2015; Naab & Ostriker 2017; Grisdale et al. 2017; Ohlin et al. 2019), again notably in dense environments such as mergers and in dense, clumpy galaxies at cosmic noon (Beraldo e Silva et al. 2020; Rathjen et al. 2023). Sub-grid recipes for stellar feedback, often calibrated on detailed observations of the Solar neighborhood, may not be equally adequate for a wider range of physical conditions (density, pressure, porosity, turbulence), and thus for a wider diversity of star formation regimes. Martin et al. (2025) noted significant discrepancies between the structures and star formation histories of galaxies in NEWHORIZON and Illustris TNG50 (Pillepich et al. 2019), and argued that differences in feedback implementations could explain these variations (see also Mercado et al. 2025, on the FIREBOX simulation). In particular, pre-supernova feedback (missing in NEWHORIZON), and small-scale coupling with the ISM (absent in TNG50) are known to play an important role in the structure of the ISM and the regulation of gas consumption. Other ingredients of feedback, including cosmic rays, have also been shown to influence the large-scale galactic properties (Martin-Alvarez et al. 2023; Bieri et al. 2026).

In conclusion, employing sub-grid models for star formation and feedback that do not fully account for the diversity of physical conditions and environments necessarily leads to a homogenization of the resulting star formation activity. However, the existence of various modes of star formation is captured in the simulation and in our analysis, including variations across cosmic time (see also Kraljic et al. 2024, in the context of the evolution of the Kennicutt–Schmidt relation). This suggests that the qualitative scenario we propose is robust, although the timescales and stochasticity of these modes may vary when adopting a different recipe. Improving current models toward a framework that treats the diversity of environmental conditions across galaxies and cosmic time remains a complex task, owing to the enormous range of scales involved.

6. CONCLUSION

The detection of galaxies with starburst-like properties (e.g., compact star formation and short depletion time) within the main sequence of galaxy formation raises questions on the diversity of star formation regimes and the transition between them. By analyzing the population of these SBMS galaxies in the cosmo-

logical simulation NEWHORIZON, we test and complement the hypotheses derived from large observational surveys. Our main findings are as follows.

- The SBMS regime exists at all redshifts ($z < 6$), and the fraction of galaxies concerned remains approximately constant ($\approx 5\%$). Along its lifetime, a galaxy can experience multiple SBMS episodes, such that, at low redshift, the majority of galaxies have been through at least one SBMS phase.
- SBMS galaxies experience more numerous and more frequent major and minor mergers, and (on average) encounter more massive companions than any other class of galaxies, possibly because of a peculiar location in the cosmic web. Their depletion time is significantly shorter than that of the other galaxies when averaging over the entire lifetime, but also during the merger-induced starburst phases only. As a result, the SBMS galaxies assemble their stellar mass early via accretion of their neighboring galaxies and merger-triggered starbursts. This precocious build-up of their stellar component favors their location within the main sequence (via a moderate sSFR).
- Examining individual cases reveals highly stochastic evolutions caused by rapidly changing SFRs, without the possibility of identifying a representative, general evolutionary track in the M_* -SFR plane.
- The SBMS phase comprises a diversity of evolutionary paths. Contrary to hypotheses in the literature, the SBMS regime denotes a slowing down of the star formation activity (from starburst to main sequence, and possibly toward quenching) for at most 25% of the galaxies. Instead, most galaxies, especially the most massive ones, return to their previous regime after a short SBMS episode (≈ 30 Myr).
- The compaction of the star-forming gas phase detected in the context of SBMS episodes leads to an increase in the SFR, but not a significant decrease in the depletion time. Such events only concern galaxies transitioning from the main sequence to starbursts.

Despite being short-lived, SBMS episodes mark important transitions along the evolution of galaxies. Their role in compaction toward quenching of star formation seems however to concern only a quarter of the galaxies. Instead, our scenario underlines the importance of a precocious assembly of the stellar mass by early mergers and merger-triggered starbursts. However, our work highlights a diversity and complexity of cases, subject to rapid variations. Establishing general evolutionary tracks for galaxies in a M_* -SFR diagram appears challenging and not representative of individual histories. We strongly suspect that the same assessment could be made when focusing on other phases of galaxy evolution, notably when considering the diversity of physical conditions leading to quenching.

Acknowledgements. CA acknowledges support from the Interdisciplinary Thematic Institute IRMIA++ within the framework of the French Investments for the Future Program. We acknowledge access to the HPC Infinity Cluster hosted at the Institut d’Astrophysique de Paris and managed by S. Rouberol.

REFERENCES

- Accard, C., Béthermin, M., Boquien, M., et al. 2025, *A&A*, 702, A206
- Agertz, O. & Kravtsov, A. V. 2015, *ApJ*, 804, 18
- Arango-Toro, R. C., Ilbert, O., Ciesla, L., et al. 2025, *A&A*, 696, A159
- Aubert, D., Pichon, C., & Colombi, S. 2004, *MNRAS*, 352, 376
- Barro, G., Faber, S. M., Pérez-González, P. G., et al. 2014, *ApJ*, 791, 52
- Beraldo e Silva, L., Debattista, V. P., Khachatryan, T., & Nidever, D. 2020, *MNRAS*, 492, 4716
- Bieri, R., Pakmor, R., van de Voort, F., et al. 2026, *MNRAS*[arXiv:2509.07124]
- Birnboim, Y. & Dekel, A. 2003, *MNRAS*, 345, 349
- Caplar, N. & Tacchella, S. 2019, *MNRAS*, 487, 3845
- Carniani, S., D’Eugenio, F., Ji, X., et al. 2025, *A&A*, 696, A87
- Carvajal-Bohorquez, C., Ciesla, L., Laporte, N., et al. 2025, arXiv e-prints, arXiv:2507.13160
- Casey, C. M., Akins, H. B., Shuntov, M., et al. 2024, *ApJ*, 965, 98
- Christensen, C. R., Davé, R., Governato, F., et al. 2016, *ApJ*, 824, 57
- Ciesla, L., Elbaz, D., & Fensch, J. 2017, *A&A*, 608, A41
- Ciesla, L., Gómez-Guijarro, C., Buat, V., et al. 2023, *A&A*, 672, A191
- Conroy, C. 2013, *ARA&A*, 51, 393
- Cortijo-Ferrero, C., González Delgado, R. M., Pérez, E., et al. 2017, ArXiv e-prints [arXiv:1702.06544]
- Cox, T. J., Jonsson, P., Somerville, R. S., Primack, J. R., & Dekel, A. 2008, *MNRAS*, 384, 386
- Daddi, E., Delvecchio, I., Dimauro, P., et al. 2022, *A&A*, 661, L7
- Daddi, E., Dickinson, M., Morrison, G., et al. 2007, *ApJ*, 670, 156
- Dalgarno, A. & McCray, R. A. 1972, *ARA&A*, 10, 375
- Dekel, A. & Birnboim, Y. 2006, *MNRAS*, 368, 2
- Dekel, A. & Burkert, A. 2014, *MNRAS*, 438, 1870
- Di Matteo, P., Bournaud, F., Martig, M., et al. 2008, *A&A*, 492, 31
- Dubois, Y., Beckmann, R., Bournaud, F., et al. 2021, *A&A*, 651, A109
- Dubois, Y., Devriendt, J., Slyz, A., & Teyssier, R. 2010, *MNRAS*, 409, 985
- Dubois, Y., Volonteri, M., Silk, J., Devriendt, J., & Slyz, A. 2014, *MNRAS*, 440, 2333
- Elbaz, D., Daddi, E., Le Borgne, D., et al. 2007, *A&A*, 468, 33
- Elbaz, D., Dickinson, M., Hwang, H. S., et al. 2011, *A&A*, 533, A119
- Elbaz, D., Leiton, R., Nagar, N., et al. 2018, *A&A*, 616, A110
- Ellison, S., Ferreira, L., Bickley, R., et al. 2025, *The Open Journal of Astrophysics*, 8, 12
- Ellison, S. L., Patton, D. R., Simard, L., & McConnachie, A. W. 2008, *AJ*, 135, 1877
- Fabian, A. C. 2012, *ARA&A*, 50, 455
- Federrath, C. & Klessen, R. S. 2012, *ApJ*, 761, 156
- Fensch, J., Renaud, F., Bournaud, F., et al. 2017, *MNRAS*, 465, 1934
- Franco, M., Elbaz, D., Zhou, L., et al. 2020, *A&A*, 643, A30
- Gómez-Guijarro, C., Elbaz, D., Xiao, M., et al. 2022, *A&A*, 659, A196
- Grisdale, K., Agertz, O., Renaud, F., et al. 2019, *MNRAS*, 486, 5482
- Grisdale, K., Agertz, O., Romeo, A. B., Renaud, F., & Read, J. I. 2017, *MNRAS*, 466, 1093
- Gui, Y., Xu, D., Wang, H., et al. 2025, arXiv e-prints, arXiv:2512.00151
- Haardt, F. & Madau, P. 1996, *ApJ*, 461, 20
- Hennebelle, P. & Chabrier, G. 2011, *ApJ*, 743, L29
- Hopkins, P. F., Cox, T. J., Hernquist, L., et al. 2013, *MNRAS*, 430, 1901
- Iyer, K. & Gawiser, E. 2017, *ApJ*, 838, 127
- Jiménez-Andrade, E. F., Magnelli, B., Karim, A., et al. 2019, *A&A*, 625, A114
- Karl, S. J., Naab, T., Johansson, P. H., et al. 2010, *ApJ*, 715, L88
- Kimm, T. & Cen, R. 2014, *ApJ*, 788, 121
- Kraljic, K., Renaud, F., Dubois, Y., et al. 2024, *A&A*, 682, A50
- Krumholz, M. R. & McKee, C. F. 2005, *ApJ*, 630, 250
- Lapiner, S., Dekel, A., Freundlich, J., et al. 2023, *MNRAS*, 522, 4515
- Le Bail, A., Daddi, E., Elbaz, D., et al. 2024, *A&A*, 688, A53
- Lee, Y.-N. & Hennebelle, P. 2016, *A&A*, 591, A31
- Leja, J., Carnall, A. C., Johnson, B. D., Conroy, C., & Speagle, J. S. 2019, *ApJ*, 876, 3
- Leys, C., Klein, O., Bernard, P., & Licata, L. 2013, *Journal of Experimental Social Psychology*, 49, 764
- Li, H., Vogelsberger, M., Bryan, G. L., et al. 2022, *MNRAS*, 514, 265
- Liu, Z., Silverman, J. D., Daddi, E., et al. 2025, *MNRAS*, 542, 397
- Lotz, J. M., Jonsson, P., Cox, T. J., et al. 2011, *ApJ*, 742, 103
- Lower, S., Narayanan, D., Leja, J., et al. 2020, *ApJ*, 904, 33
- Lyu, Y., Magnelli, B., Elbaz, D., et al. 2025, *A&A*, 693, A313
- Magnelli, B., Gómez-Guijarro, C., Elbaz, D., et al. 2023, *A&A*, 678, A83
- Mancini, C., Daddi, E., Juneau, S., et al. 2019, *MNRAS*, 489, 1265
- Martin, G., Jackson, R. A., Kaviraj, S., et al. 2021, *MNRAS*, 500, 4937
- Martin, G., Watkins, A. E., Dubois, Y., et al. 2025, *MNRAS*, 541, 1831
- Martin-Alvarez, S., Sijacki, D., Haehnelt, M. G., et al. 2023, *MNRAS*, 525, 3806
- Mercado, F. J., Moreno, J., Feldmann, R., et al. 2025, *ApJ*, 983, 93
- Mihos, J. C. & Hernquist, L. 1994, *ApJ*, 431, L9
- Mihos, J. C. & Hernquist, L. 1996, *ApJ*, 464, 641
- Mineo, S., Rappaport, S., Levine, A., et al. 2014, *ApJ*, 797, 91
- Moreno, J., Torrey, P., Ellison, S. L., et al. 2021, *MNRAS*, 503, 3113
- Müller, J. 2000, *Journal of Research of the National Institute of Standards and Technology*, 105, 551
- Muratov, A. L., Kereš, D., Faucher-Giguère, C.-A., et al. 2015, *MNRAS*, 454, 2691
- Naab, T. & Ostriker, J. P. 2017, *ARA&A*, 55, 59

- Noeske, K. G., Weiner, B. J., Faber, S. M., et al. 2007, *ApJ*, 660, L43
- Ocvirk, P., Pichon, C., Lançon, A., & Thiébaud, E. 2006, *MNRAS*, 365, 74
- Ohlin, L., Renaud, F., & Agertz, O. 2019, *MNRAS*, 485, 3887
- O’Leary, J. A., Moster, B. P., Naab, T., & Somerville, R. S. 2021, *MNRAS*, 501, 3215
- Padoan, P. & Nordlund, Å. 2011, *ApJ*, 730, 40
- Pan, H.-A., Lin, L., Hsieh, B.-C., et al. 2019, *ApJ*, 881, 119
- Peng, Y.-j., Lilly, S. J., Kovač, K., et al. 2010, *ApJ*, 721, 193
- Perret, V., Renaud, F., Epinat, B., et al. 2014, *A&A*, 562, A1
- Pillepich, A., Nelson, D., Springel, V., et al. 2019, *MNRAS*, 490, 3196
- Popesso, P., Concas, A., Cresci, G., et al. 2023, *MNRAS*, 519, 1526
- Puglisi, A., Daddi, E., Liu, D., et al. 2019, *ApJ*, 877, L23
- Puglisi, A., Daddi, E., Valentino, F., et al. 2021, *MNRAS*, 508, 5217
- Rathjen, T.-E., Naab, T., Walch, S., et al. 2023, *MNRAS*, 522, 1843
- Renaud, F., Bournaud, F., Agertz, O., et al. 2019a, *A&A*, 625, A65
- Renaud, F., Bournaud, F., Daddi, E., & Weiß, A. 2019b, *A&A*, 621, A104
- Renaud, F., Bournaud, F., Emsellem, E., et al. 2013, *MNRAS*, 436, 1836
- Renaud, F., Bournaud, F., Kraljic, K., & Duc, P.-A. 2014, *MNRAS*, 442, L33
- Renaud, F., Segovia Otero, Á., & Agertz, O. 2022, *MNRAS*, 516, 4922
- Rodighiero, G., Daddi, E., Baronchelli, I., et al. 2011, *ApJ*, 739, L40
- Romeo, A. B., Agertz, O., & Renaud, F. 2023, *MNRAS*, 518, 1002
- Rosdahl, J. & Blaizot, J. 2012, *MNRAS*, 423, 344
- Rosolowsky, E., Hughes, A., Leroy, A. K., et al. 2021, *MNRAS*, 502, 1218
- Schreiber, C., Pannella, M., Elbaz, D., et al. 2015, *A&A*, 575, A74
- Schweizer, F. 2005, in *ASSL Vol. 329: Starbursts: From 30 Doradus to Lyman Break Galaxies*, 143
- Segovia Otero, Á., Agertz, O., Renaud, F., et al. 2025, *MNRAS*, 538, 2646
- Segovia Otero, Á., Renaud, F., & Agertz, O. 2022, *MNRAS*, 516, 2272
- Speagle, J. S., Steinhardt, C. L., Capak, P. L., & Silverman, J. D. 2014, *ApJS*, 214, 15
- Sutherland, R. S. & Dopita, M. A. 1993, *ApJS*, 88, 253
- Tacchella, S., Dekel, A., Carollo, C. M., et al. 2016, *MNRAS*, 457, 2790
- Tacchella, S., Forbes, J. C., & Caplar, N. 2020, *MNRAS*, 497, 698
- Tacconi, L. J., Genzel, R., & Sternberg, A. 2020, *ARA&A*, 58, 157
- Tadaki, K.-i., Belli, S., Burkert, A., et al. 2020, *ApJ*, 901, 74
- Tan, Q.-H., Daddi, E., Magnelli, B., et al. 2024, *Nature*, 636, 69
- Tarrasse, M., Gómez-Guijarro, C., Elbaz, D., et al. 2025, *A&A*, 697, A181
- Teyssier, R. 2002, *A&A*, 385, 337
- Teyssier, R., Chapon, D., & Bournaud, F. 2010, *ApJ*, 720, L149
- Teyssier, R., Moore, B., Martizzi, D., Dubois, Y., & Mayer, L. 2011, *MNRAS*, 414, 195
- Tsuge, K., Sano, H., Tachihara, K., et al. 2020, *arXiv e-prints*, arXiv:2010.08816
- Tweed, D., Devriendt, J., Blaizot, J., Colombi, S., & Slyz, A. 2009, *A&A*, 506, 647
- Whitaker, K. E., Franx, M., Leja, J., et al. 2014, *ApJ*, 795, 104
- Whitmore, B. C., Chandar, R., Schweizer, F., et al. 2010, *AJ*, 140, 75
- Xu, C. K., Lisenfeld, U., Gao, Y., & Renaud, F. 2021, *ApJ*, 918, 55
- Zhang, Z., Zhang, X., Li, H., et al. 2025, *ApJ*, 991, 170

APPENDIX A: EXAMPLES OF EVOLUTIONARY TRACKS OF SBMS GALAXIES

Examining the evolution of every galaxy is beyond the scope of this paper. However, to illustrate possible paths and variations along them, Figure A.1 shows the history of two galaxies detected as SBMS at $z = 3$. The case with the lowest SFR disappears at $z \approx 2.3$ when it merges with a larger galaxy. The rapid variations of the SFR visible in these examples (and in most, if not all simulated SFRs) explain the short durations of SBMS episodes.

APPENDIX B: MERGER FREQUENCY

Figure B.1 shows that starburst and SBMS galaxies experience major mergers ≈ 1.4 time more frequently than the other galaxies. The more numerous and more frequent major merger events favor an enhanced star formation activity, and a rapid build-up of the stellar component (by accretion and accelerated in situ formation).

With the mass growth, this aspect is one of the main variation with redshift, caused by the evolution of the large-scale environment. The analysis is repeated at $z = 1$ in Figure B.2, and completed with the count of merger events in Figure B.3. As detailed in Section 4.4, the peculiarity of SBMS galaxies in terms of merger events fade with decreasing redshift, further highlighting the early and precocious nature of their assembly.

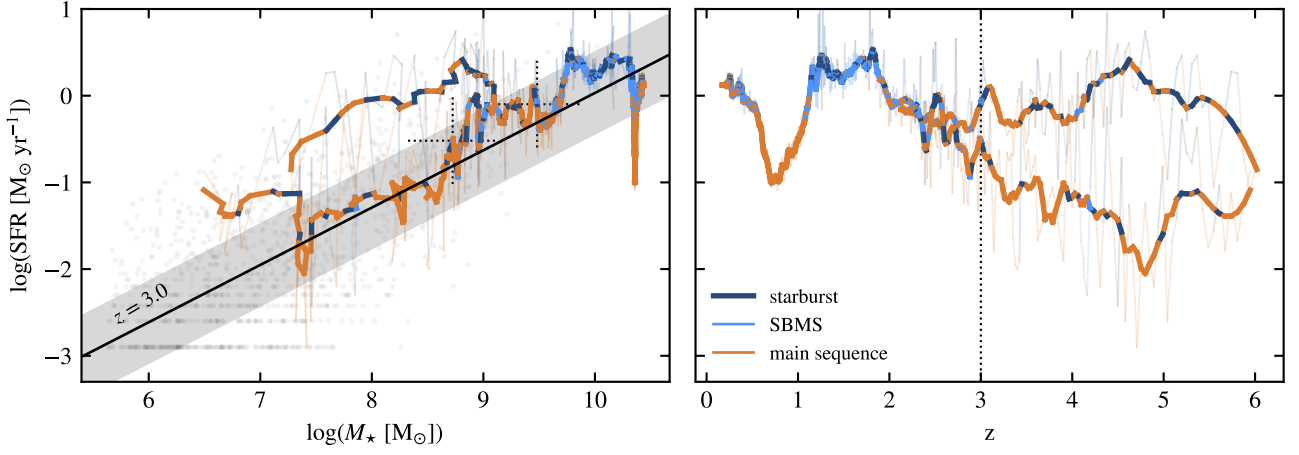


Fig. A.1. *Left panel:* Evolution of two examples of SBMS galaxies identified as such at $z = 3$ in the stellar mass-SFR plane. The positions of the galaxies at $z = 3$ are indicated by the large plus signs. *Right panel:* Evolution of the SFR as function of redshift of the same galaxies. The curves are color-coded by the category of the galaxy: SBMS in light blue, off-main sequence starburst in dark blue, and main sequence in orange. The curves have been smoothed by a Savitzky-Golay algorithm to improve readability, with the original measurements shown by the semi-transparent lines. Black dots represent the entire population of star forming galaxies at $z = 3$, with the main sequence shown with the solid line and shaded area. We remind the reader that the position of the main sequence changes with redshift: these elements in black can be used to guide the eye only at $z = 3$.

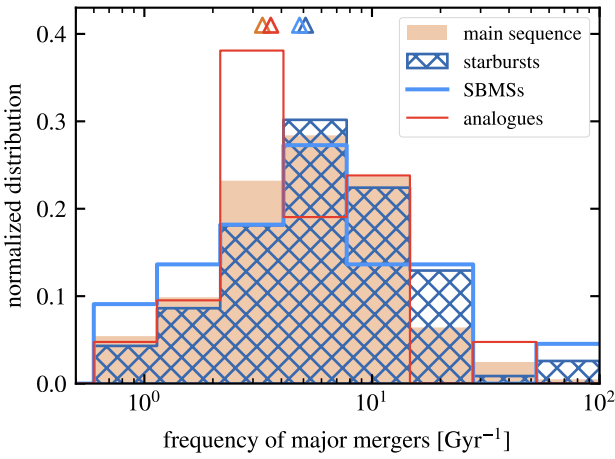


Fig. B.1. Frequency of major mergers computed as the number of major mergers divided by the lifetime of the galaxy (at $z = 3$). Triangles indicate the median value of each class.

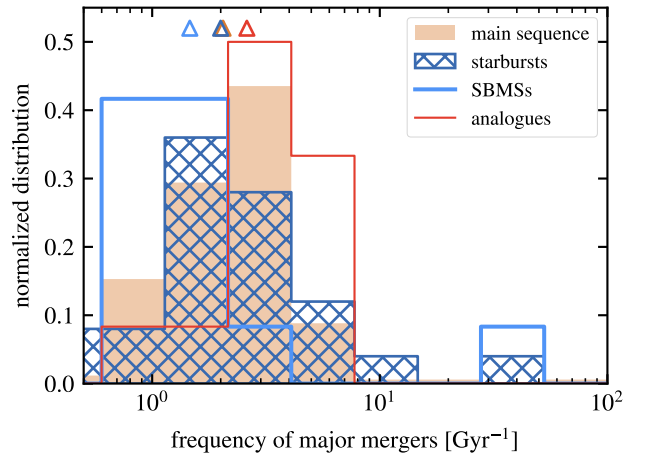


Fig. B.2. Same as Figure B.1 but at $z = 1$.

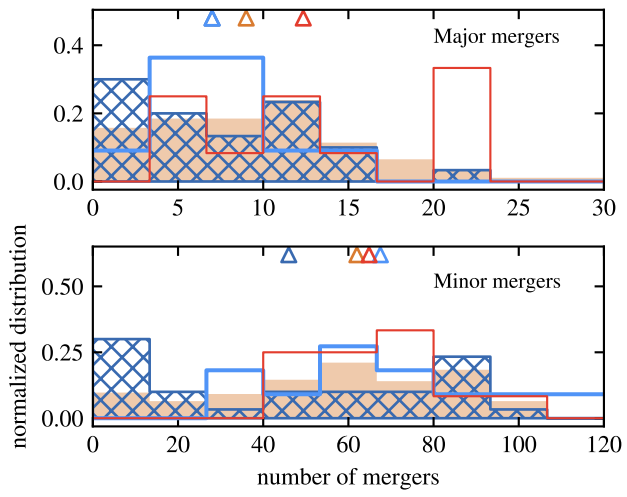


Fig. B.3. Same as Figure 8 but at $z = 1$.